Electronic Supporting Information

Highly efficient CO_2 capture and chemical fixation of a microporous (3, 36)-connected *txt*-type Cu(II)-MOF with multifunctional sites

Wenyu Dong [a], Zhaoxu Wang*[a], Zuxian Cai [a], Yiqiang Deng*[b], Guanyu Wang [a] and Baishu Zheng*[a]

[a]*Key Laboratory of Theoretical Organic Chemistry and Function Molecule of Ministry of Education, Hunan Provincial Key Laboratory of Controllable Preparation and Functional Application of Fine Polymers, Hunan Provincial Key Laboratory of Advanced Materials for New Energy Storage and Conversion, School of Chemistry and Chemical Engineering, Hunan University of Science and Technology, Xiangtan 411201, China. E-mail: zbaishu@163.com (B. S. Zheng); hunst_chem@163.com (Z. X. Wang).*

[b] *School of Chemical Engineering, Guangdong University of Petrochemical Technology, Maoming 525000, Guangdong, China. E-mail: yqdeng@gdupt.edu.cn (Y. Q. Deng).*

1. Materials and Methods

All chemical reagents were obtained from commercial sources and used without further purification unless otherwise noted. ^{1}H NMR spectra were recorded on a Bruker AVANCE III 500 MHz spectrometer with tetramethylsilane as an internal reference. The IR spectra were recorded in the 400-4000 cm^{-1} on a VECTOR TM 22 spectrometer using KBr pelts. Thermal gravimetric analysis (TGA) were performed under N_2 atmosphere (100 mL min^{-1}) with a heating rate of 5 K min^{-1} using a 2960 SDT thermogravimetric analyzer. Crystallographic data of the HNUST-17 were collected by an Apex II diffractometer with Mo/K_α radiation (λ = 0.71073 Å) at room temperature. Powder X-ray diffraction (PXRD) data were collected on a Bruker D8 ADVANCE X-ray diffractometer using Cu K_α radiation (λ = 1.5418 Å) at room temperature. Low-pressure gas adsorption-desorption isotherms were obtained using a Belsorp-mini volumetric adsorption instrument from BEL Japan Inc. High-pressure gravimetric gas adsorption-desorption measurements were performed on an BELSORP-HP adsorption analyzer (Janpan).

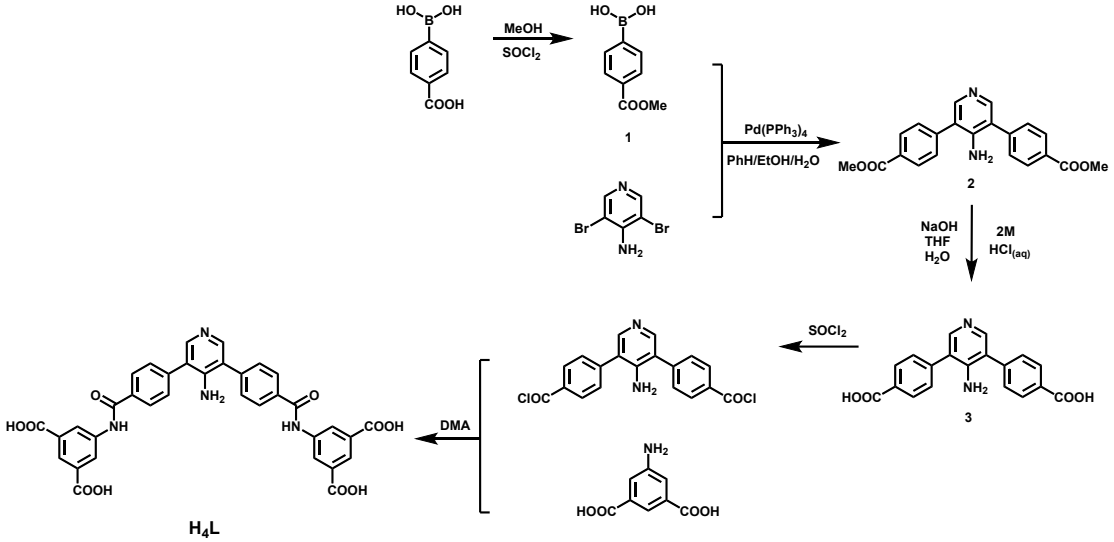

Scheme S1. Synthetic route of the organic linker, 5,5'-((4,4'-(4-aminopyridine-3,5-diyl)bis(benzoyl)bis(azanediyl))diisophthalic acid, H_4L

2. Synthesis of 4-(methoxycarbonyl)phenyl)boronic acid (1)

$SOCl_2$ (10 mL, 138 mmol) was added dropwise to a solution of 4-carboxyphenyl boric acid (1.0 g, 6.02 mmol) in 10 mL methanol, and then the solution was refluxed at 75 °C with rigorous stirring for 24 hours. After removal of excess methanol and $SOCl_2$ under vacuum, the residue was washed by water repeatedly, dried at 100 °C to give the 4-(methoxycarbonyl)phenyl)boronic acid as a white solid (0.951 g, ~95.1% yield). ^{1}H NMR (500 MHz, DMSO-d_6, δ ppm): 8.06 (s, 2H, ArH), 7.80 (s, 2H, ArH), 4.12 (s, 2H, OH), 3.89 (s, 3H, CH_3).

3. Synthesis of dimethyl 4,4'-(4-aminopyridine-3,5-diyl)dibenzoate (2)

The mixture of 3,5-dibromopyridine-4 amine (1.26 g, 5.00 mmol), $Pd(PPh_3)_4$ (0.29 g, 0.25 mmol), 4-(methoxycarbonyl)phenyl)boronic acid (2.16 g, 12 mmol), K_2CO_3 (3.32 g, 7.2 mmol) and toluene-ethanol-water (30 mL, 15 mL, 15 mL) was stirred at 75 °C for 24 hours and then cooled to room temperature. After removal of organic solvent under vacuum, the residue was dissolved in 150 mL H_2O and then extracted three times by dichloromethane (100 mL). After removal of dichloromethane

under vacuum, the residue was washed with methanol several times to give dimethyl 4,4'-(4-aminopyridine-3,5-diyl)dibenzoate as a white solid (0.666 g, ~yield 45.95%). ^{1}H NMR (500 MHz, DMSO-d_6, δ ppm): 8.23 (s, 2H, ArH), 8.04 (s, 4H, ArH), 7.68 (s, 4H, ArH), 7.15 (s, 2H, NH_2), ,3.86 (s, 6H, CH_3).

4. Synthesis of 4,4'-(4-aminopyridine-3,5-diyl)dibenzoic acid (3)

80 mL (2M) of sodium hydroxide aqueous solution was added to a solution of dimethyl 4,4-(4-aminopyridine-3,5)-benzoate (1.45 g, 4.00 mmol) in 60 mL DMF, and the solution was stirred at 60 °C for 6 hours. After removal of DMF under vacuum, the residue was dissolved in water, acidified with 12 M HCl to pH = 2~3. The precipitated solids were filtered off and repeatedly washed with water and then dried in a vacuum oven at 100 °C to give pure 4,4'-(4-aminopyridine-3,5-diyl)dibenzoic acid as a light yellow solid (0.775 g, ~yield 62.5%). ^{1}H NMR (500 MHz, DMSO-d_6, δ ppm):13.14 (broad peak, 2H, COOH), 8.22 (s, 2H, ArH), 8.09 (s, 4H, ArH), 7.65 (s, 4H, ArH), 7.16 (s, 2H, NH_2).

5. Activation of HNUST-17

The solvent-exchanged HNUST-17 was prepared by immersing the as-synthesized sample in dry acetone for 48 hours to remove the non-volatile solvates (DMF and water), the extract was decanted every 8 hours and fresh acetone was replaced. The completely activated HNUST-17 sample was obtained by heating the acetone-exchanged sample at 110 °C under a dynamic high vacuum for 24 hours. During this time, the pale blue sample changed to a deep purple-blue colour (Fig. S3), indicative of the presence of open copper(II) sites. The completely-activated samples were moisture sensitive and a few minutes of exposure to air could change the sample's color back to pale blue. Selected IR (KBr, cm^{-1}, Fig. S4): 3555, 3411, 3233, 2031, 1621, 1552, 1369, 1290, 1107, 1014, 887, 856, 782, 724, 617, 475.

6. IAST selectivity calculation

Ideal adsorbed solution theory (IAST)[S1] was used to predict binary mixture adsorption from the experimental pure-gas isotherms. To perform the integrations required by IAST, the experimental single-component isotherms was fitted by the dual-site Langmuir-Freundlich equation:

$$N = a_1 \cdot \frac{b_1 \cdot P^{1/c_1}}{1 + b_1 \cdot P^{1/c_1}} + a_2 \cdot \frac{b_2 \cdot P^{1/c_2}}{1 + b_2 \cdot P^{1/c_2}} \qquad (1)$$

Here, P is the pressure of the bulk gas at equilibrium with the adsorbed phase (kPa), N is the adsorbed amount per mass of adsorbent (mol/kg), a_1 and a_2 are the saturation capacities of sites 1 and 2 (mol/kg), b_1 and b_2 are the affinity coefficients of sites 1 and 2 (1/kPa), and c_1 and c_2 represent the deviations from an ideal homogeneous surface.

For a binary mixture of species i and j, the adsorption selectivity, S_{ads}, is defined as:

$$S_{ads} = \frac{x_i / x_j}{y_i / y_j} \qquad (2)$$

Here, S_{ads} is the adsorption selectivity. x_i and x_j, are the mole fractions of components i and j in the adsorbed phase, respectively. While y_i and y_j are the mole fractions of components i and j in the gas phase, respectively.

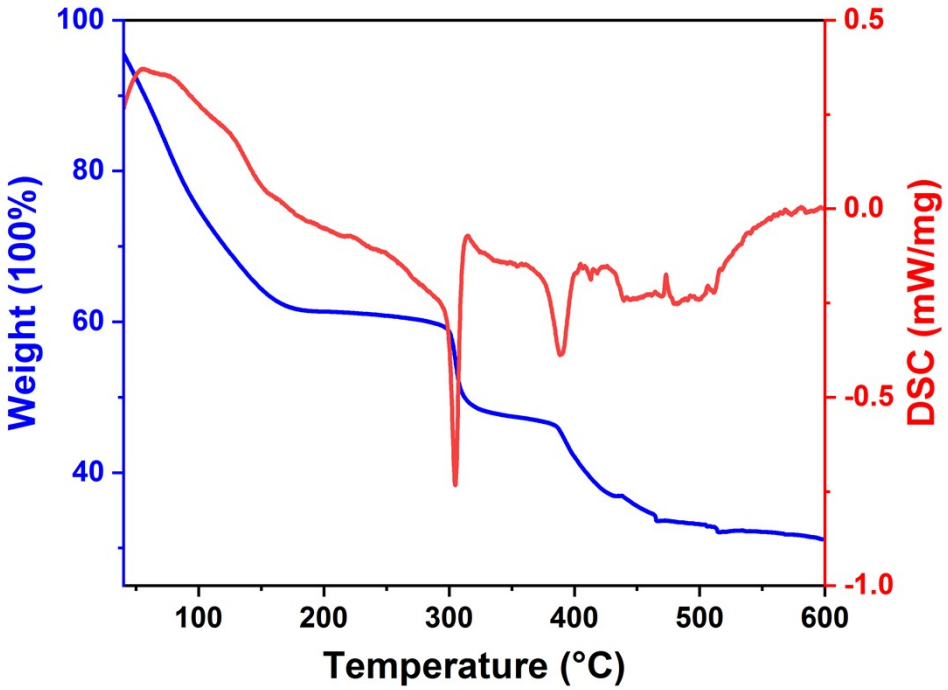

Fig. S1 TGA-DSC data of as-synthesized **HNUST-17**.

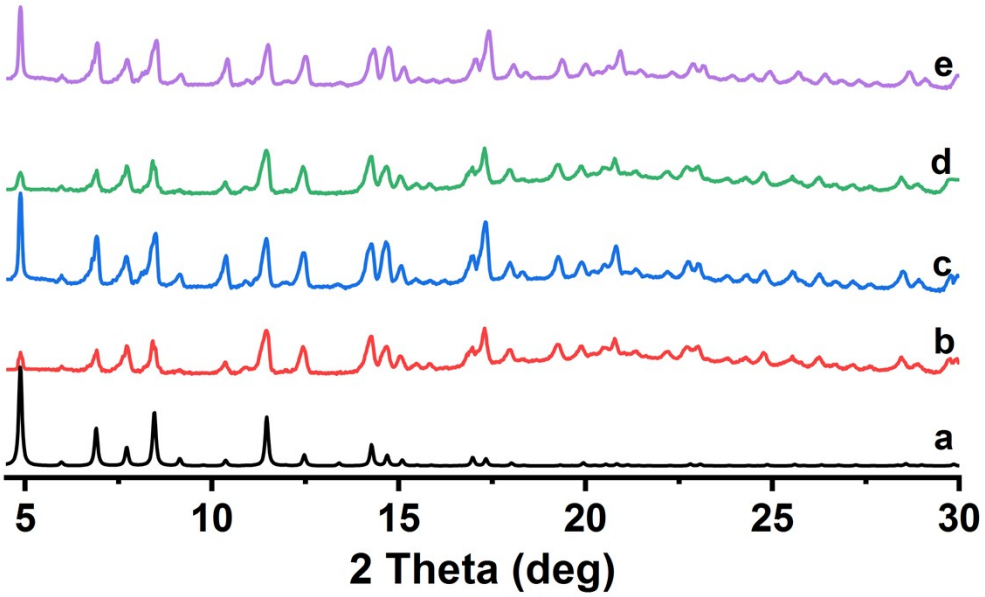

Fig. S2 PXRD patterns of HNUST-17: a) simulated, b) as-synthesized, c) activated, d) immersion in water for 2 days, and e) after the 5th cycle of catalytic reaction, respectively.

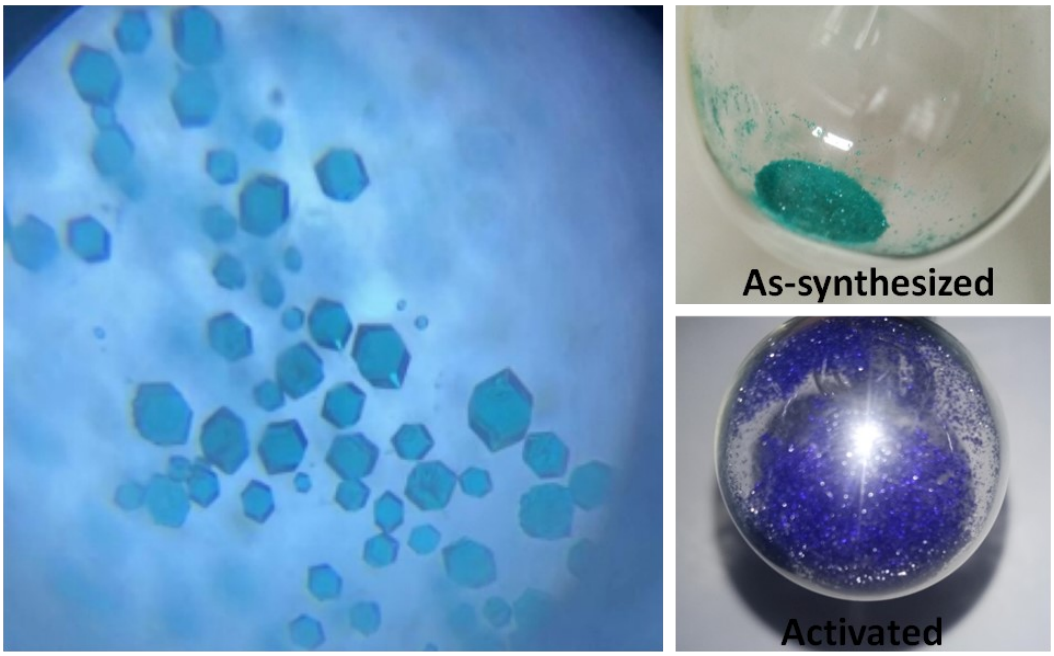

Fig. S3 Left) Photographic image of as-synthesized HNUST-17, the crystal size has been magnified about 80 times; Right) Visual color change of HNUST-17 upon activation.

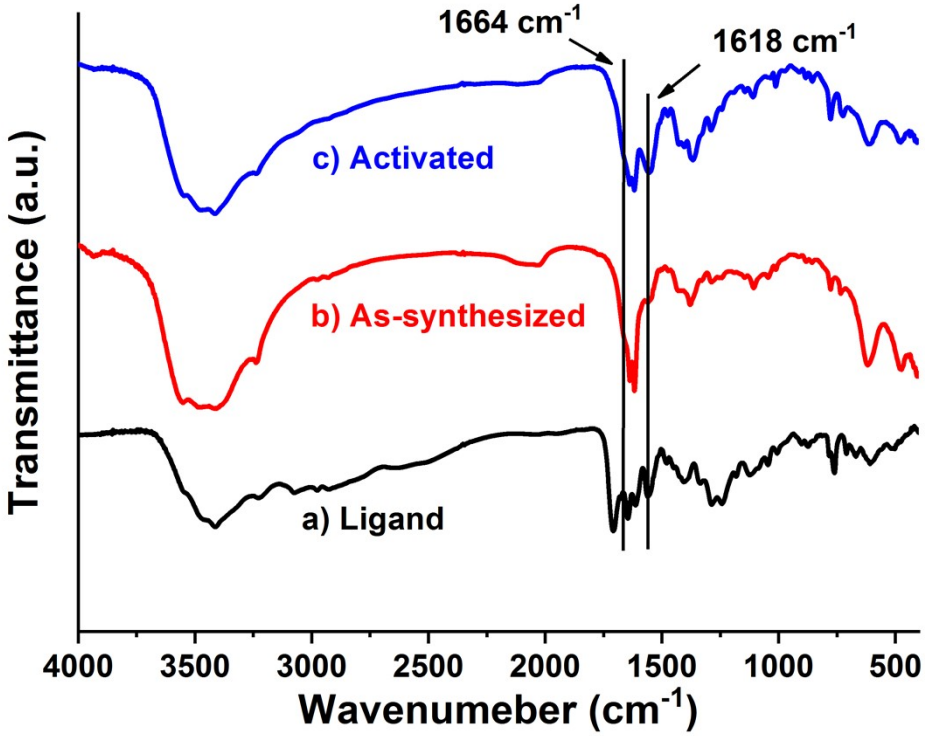

Fig. S4 The IR spectra for HNUST-17. a) Ligand; b) As-synthesized; and c) Activated HNUST-17. Note the absence of the vibration frequencies of the solvent DMF and methanol molecules in the activated samples. The presence of the *ν*(OH) stretching frequencies at 1618 cm^{-1} in activated samples may result from the rapid re-adsorption of trace moisture during the IR measurements.

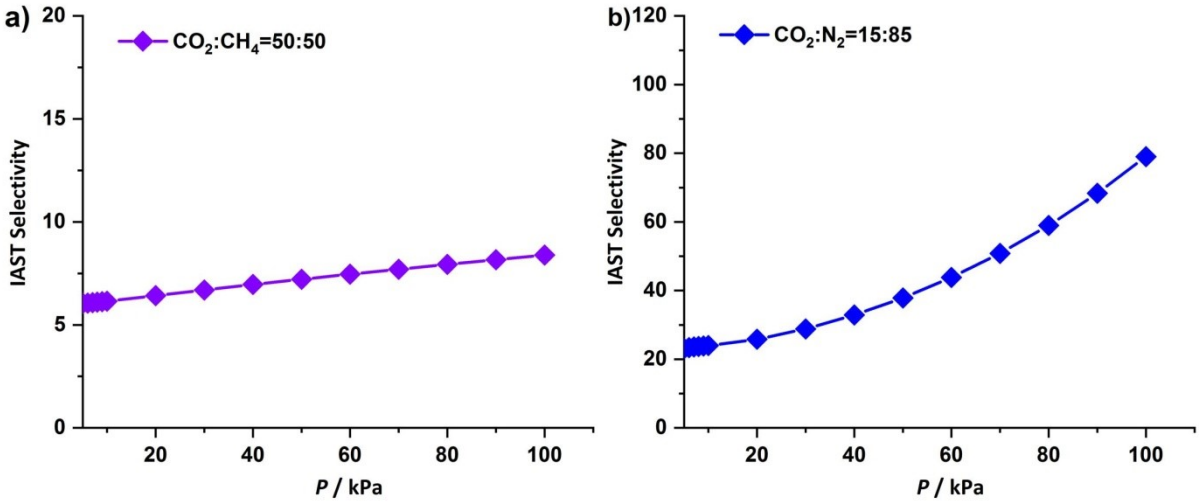

Fig. S5 IAST (Ideal Adsorbed Solution Theory) selectivity of CO_2/CH_4 and CO_2/N_2 for HNUST-17 at 273 K under 1 bar. HNUST-17 shows a moderate CO_2/CH_4 selectivity of 8.4 for CO_2-CH_4 (50:50) binary mixtures, and high CO_2/N_2 selectivity with value of 79 for CO_2-N_2 (15:85) binary mixtures at 273 K and 1 bar, respectively.

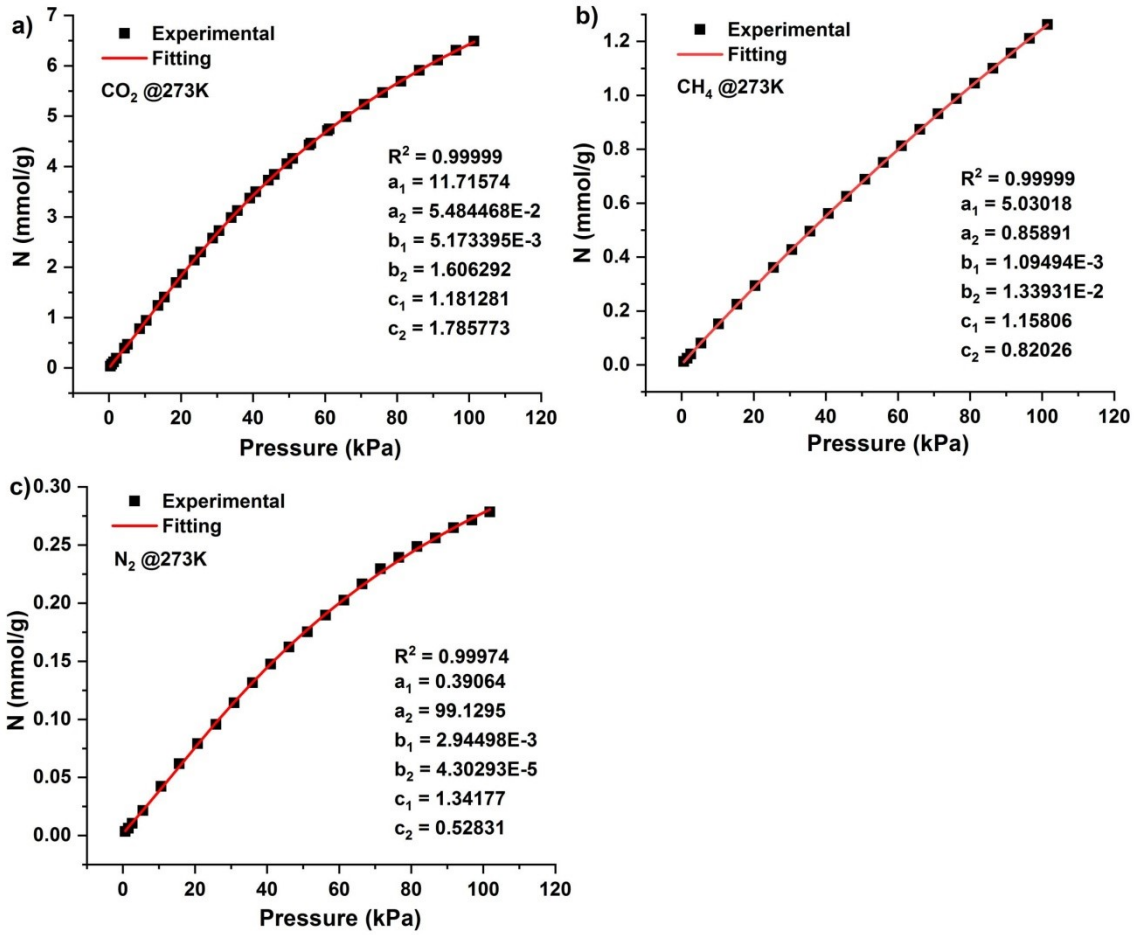

Fig. S6 a-c) Details of dual-site Langmuir-Freundlich equation (solid lines) fitting to the experimental CO_2, CH_4 and N_2 adsorption data (symbols) for HNUST-17 collected at 273 K, respectively. Note: The R^2 values for all the fitted isotherms were over 0.99974. Hence, the fitted isotherm parameters were applied to perform the integrations in IAST.

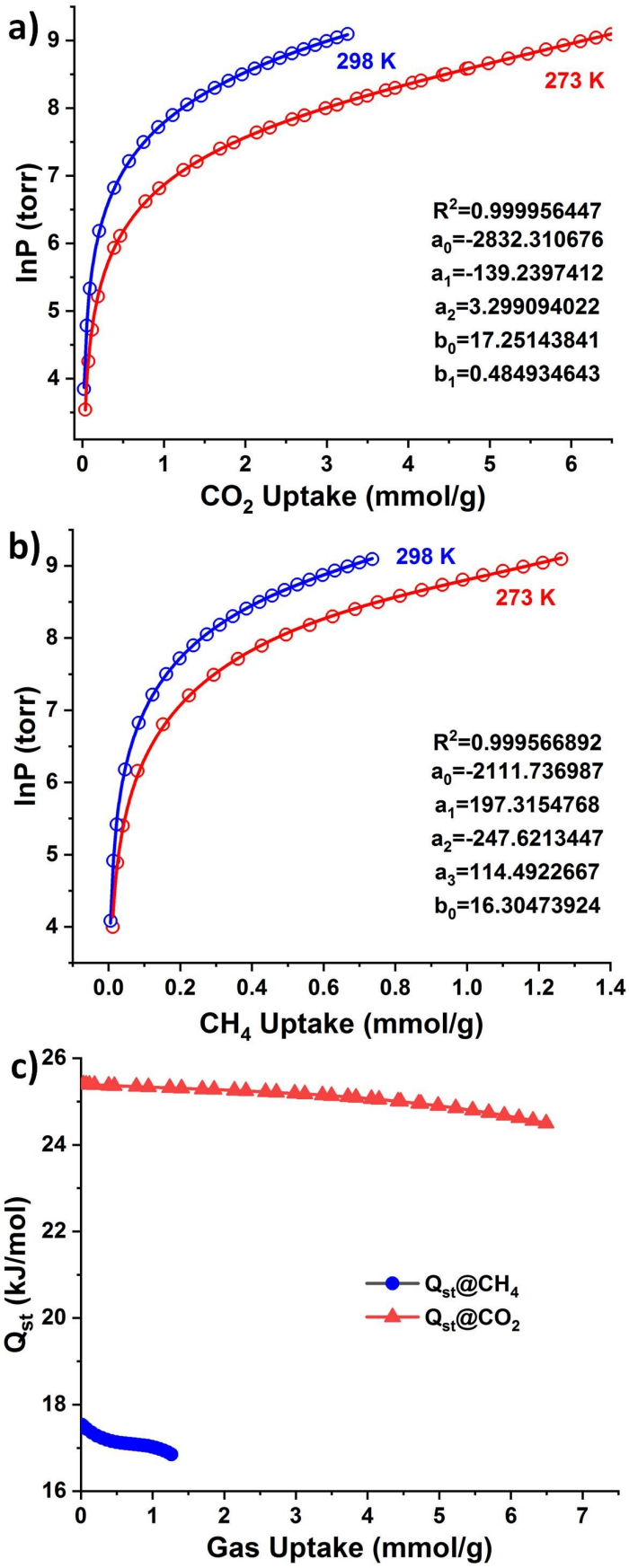

Fig. S7 a-b) Details of Virial equation (symbols) fitting to the experimental CO_2 and CH_4 adsorption data (solid lines) for HNUST-17 collected at 273 K and 298 K; c) The CO_2 and CH_4 isosteric adsorption enthalpies of HNUST-17.

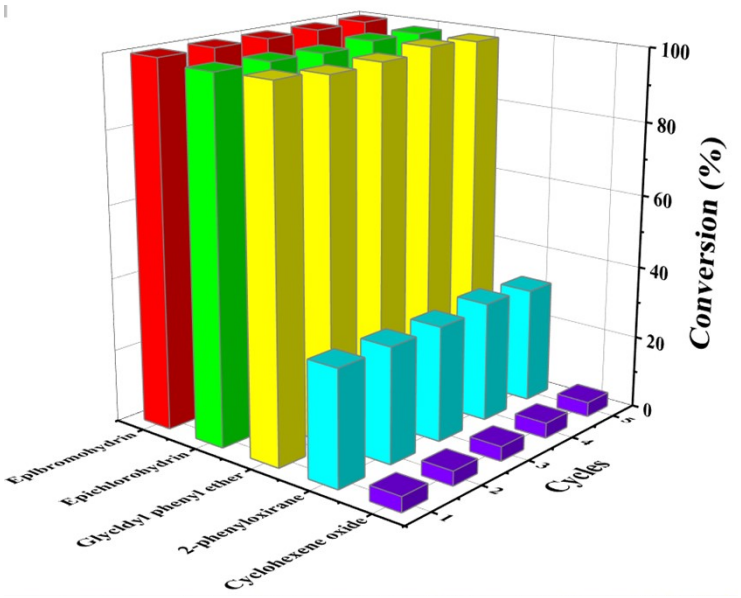

Fig. S8 Recycle experiments of HNUST-17 for the cycloaddition of CO_2 with various epoxides at 80 °C and 1 bar pressure of CO_2.

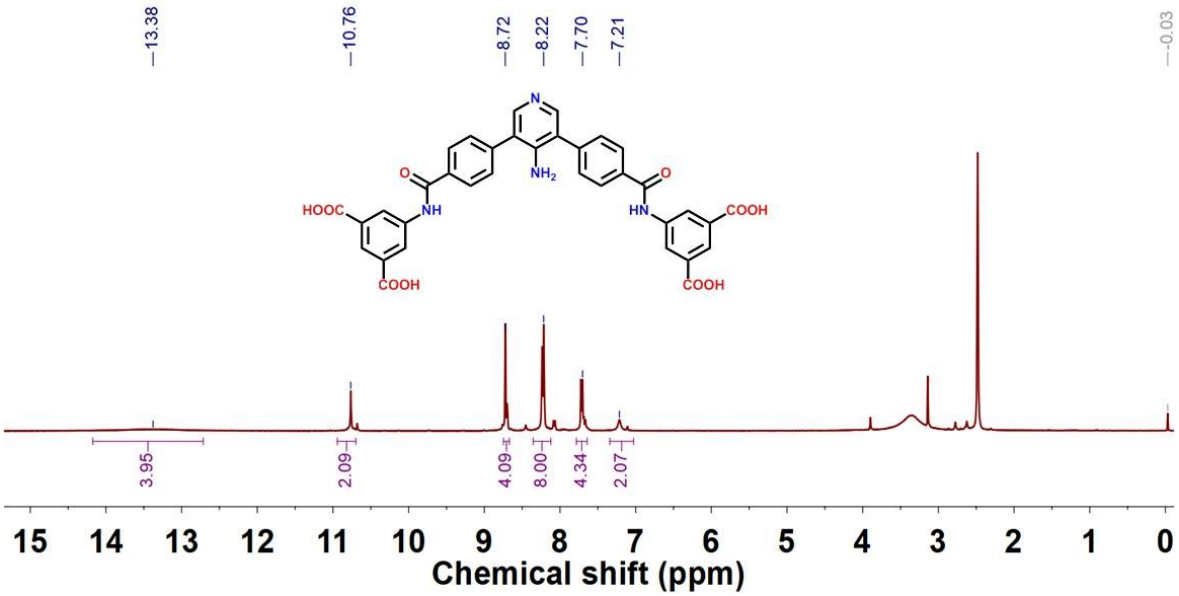

Fig. S9 The ^{1}H NMR spectrum of the organic linker, 5,5'-((4,4'-(4-aminopyridine-3,5-diyl)bis-(benzoyl))bis(azanediyl))diisophthalic acid, H_4L.

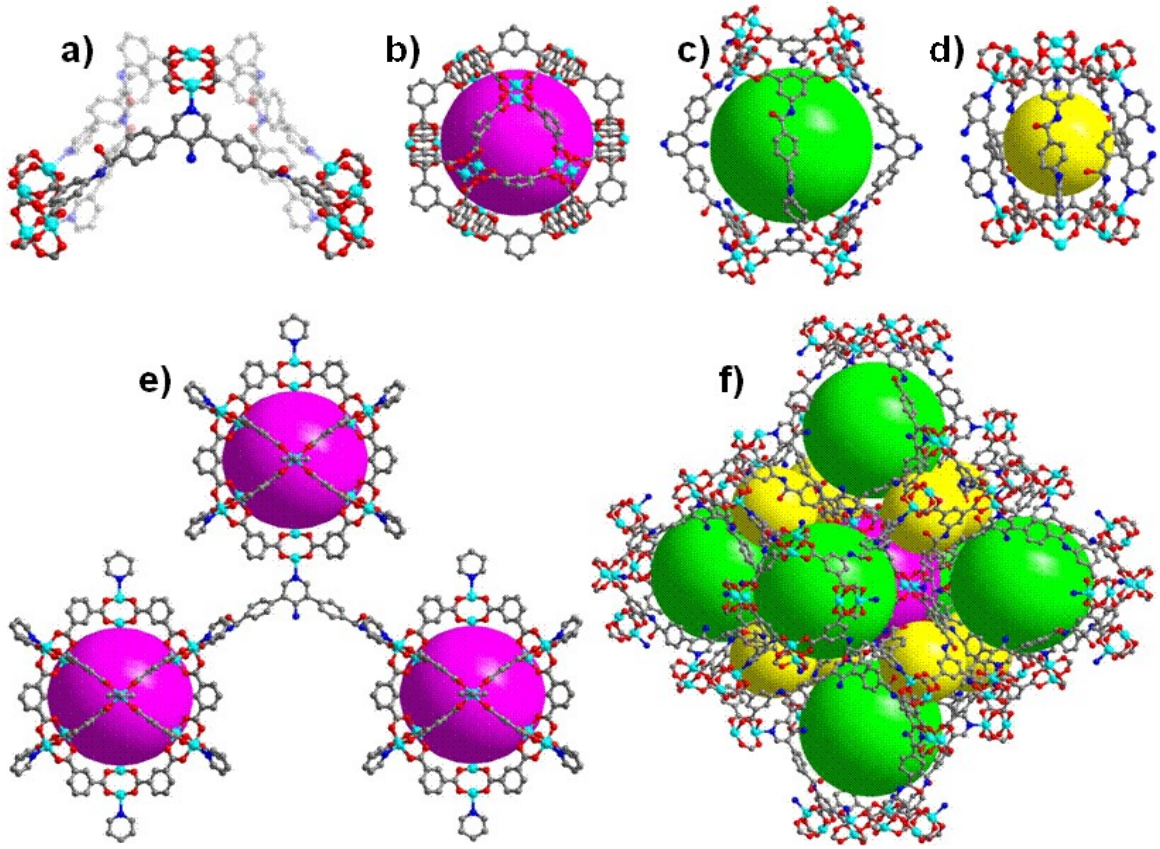

Fig. S10 Crystal structure of HNUST-17. a) Coordination environment of the dicopper(II) paddlewheel clusters and ligands. b-d) Cage A (cuboctahedron) and Cages B-C in the framework. e-f) Schematic (3, 36)-connected txt topological structure. Cu, blue-green; C, black; O, red; N, blue. Water molecules and H atoms have been omitted for clarity.

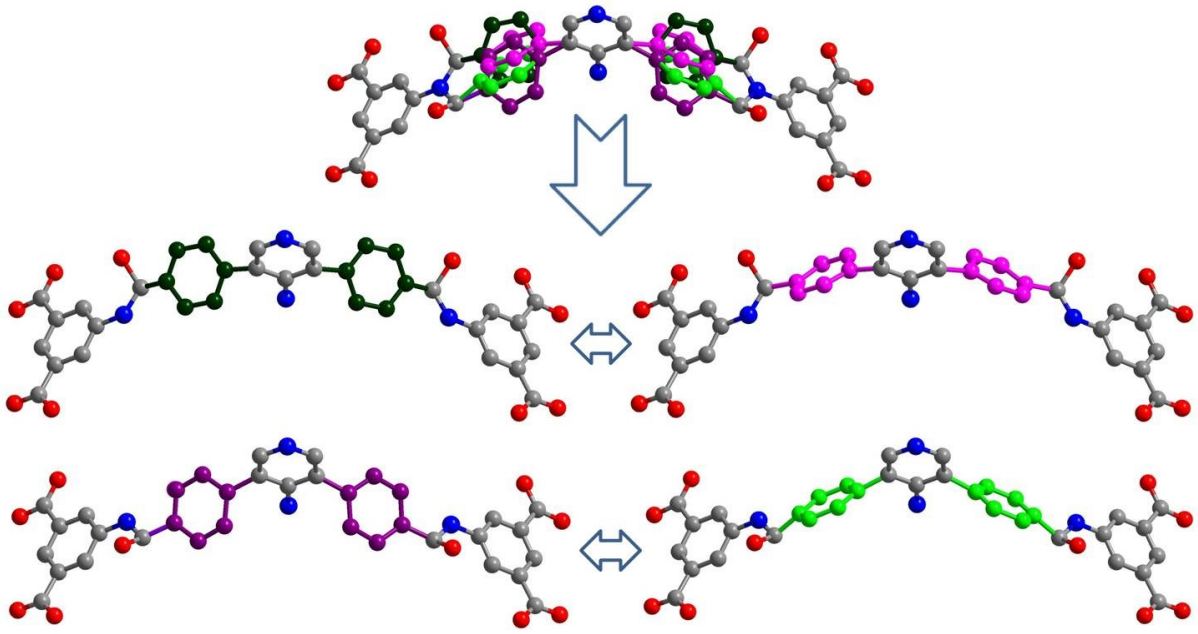

Fig. S11 The acylamide and benzene moieties of the H_4L linker in the crystal structure of HNUST-17 are disordered over two and four positions with equal probability, respectively. Only the *cis*-structures of the amide moieties in ligand are showed in above illustrations.

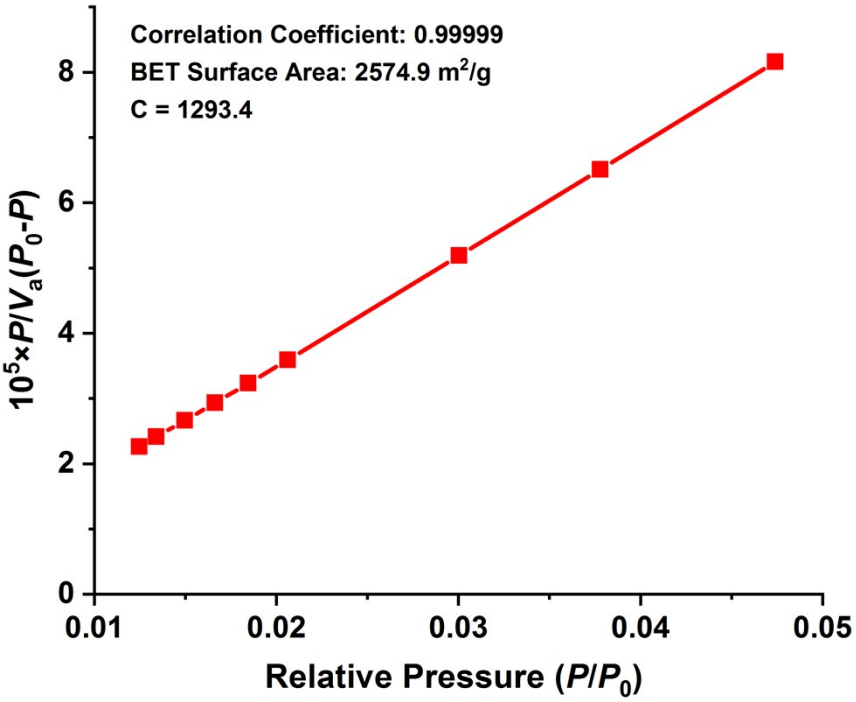

Fig. S12 The BET plots for HNUST-17 in the chosen range (P/P_0 = 0.01-0.05). This range was chosen according to two major criteria established in literatures[S2-3]: (1) The pressure range selected should have values of $Q(P_0\text{-}P)$ increasing with P/P_0. (2) The y intercept of the linear region must be positive to yield a meaningful value of the C parameter, which should be greater than zero.

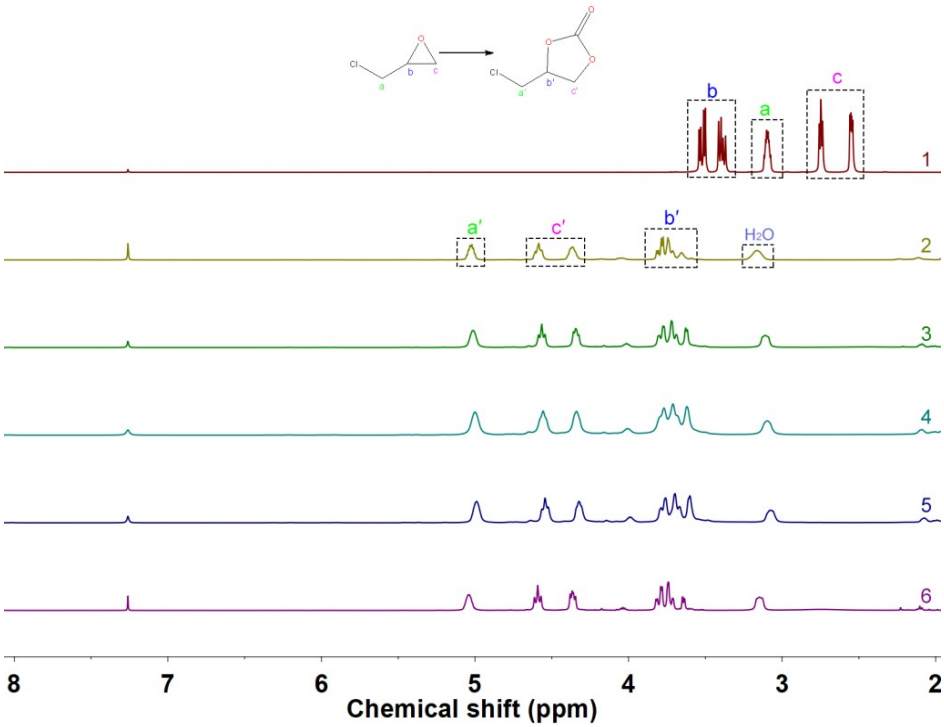

Fig. S13 The ^1H NMR spectrum (in $CDCl_3$) of a solution after the cycloaddition of CO_2 with 2-

(chloromethyl)oxirane: 1) without catalyst HNUST-17, 2) first cycle, 3) second cycle, 4) third cycle, 5) fourth cycle and 6) fifth cycle. The yields of the reaction have been calculated by integration of cyclic carbonates protons at the end of the reaction, due to the distinct chemical shifts for the corresponding epoxide protons.

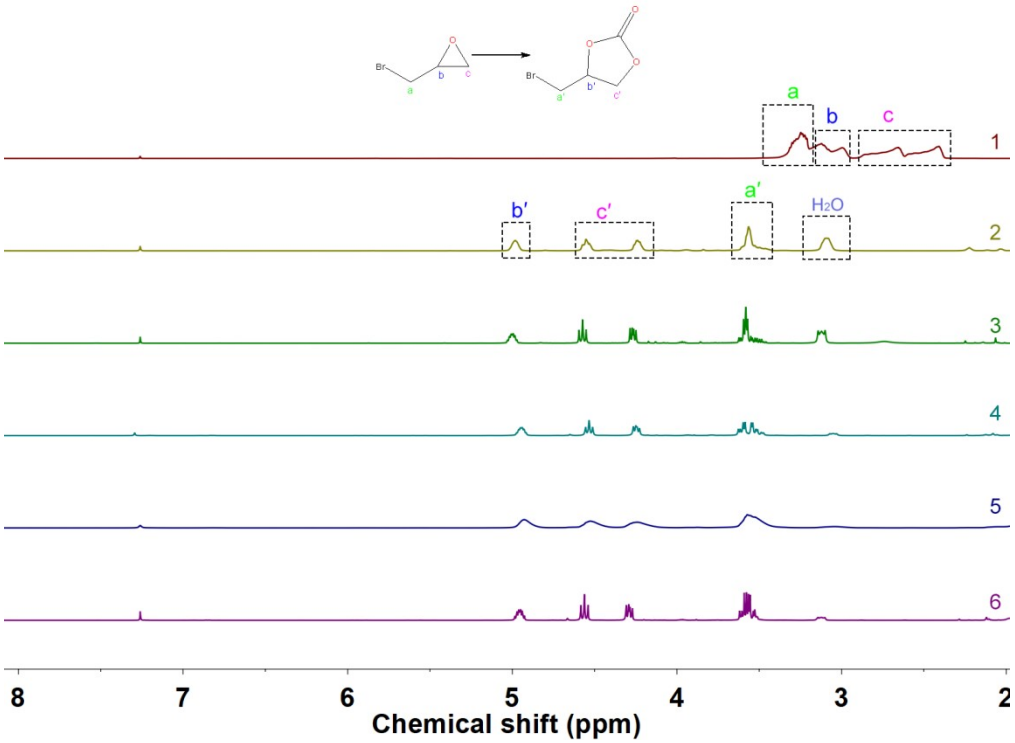

Fig. S14 The ^{1}H NMR spectrum (in $CDCl_3$) of a solution after the cycloaddition of CO_2 with 2-(bromomethyl)oxirane: 1) without catalyst HNUST-17, 2) first cycle, 3) second cycle, 4) third cycle, 5) fourth cycle and 6) fifth cycle.

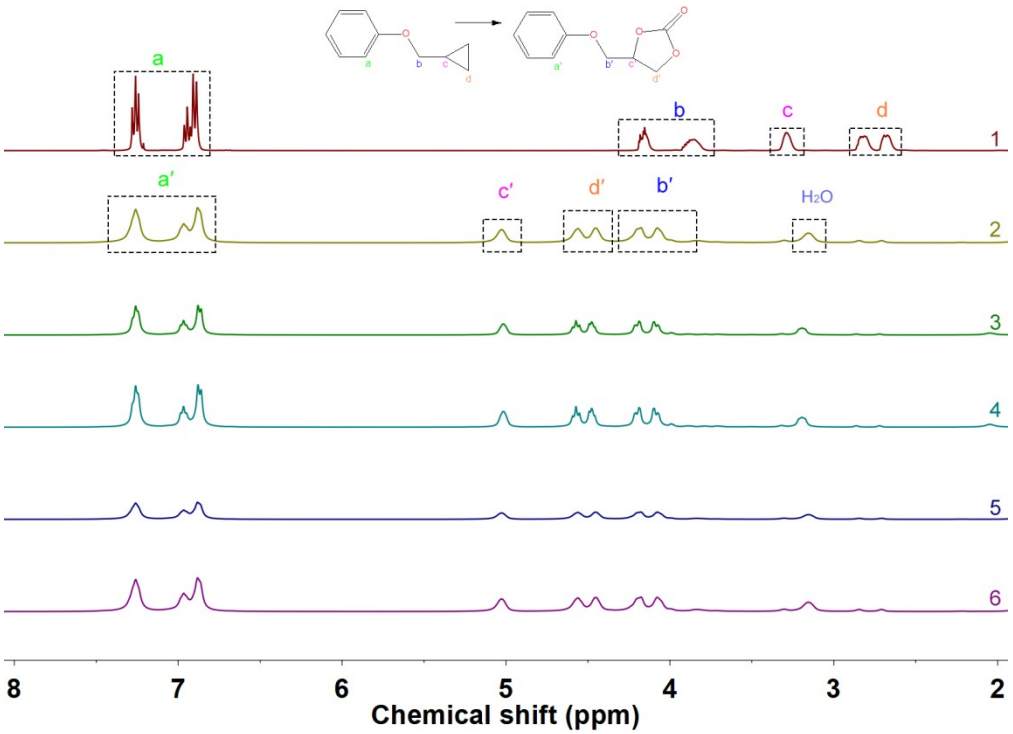

Fig. S15 The ^{1}H NMR spectrum (in $CDCl_3$) of a mixture after the cycloaddition of CO_2 with 2-(phenoxymethyl)oxirane: 1) without catalyst HNUST-17, 2) first cycle, 3) second cycle, 4) third cycle, 5) fourth cycle and 6) fifth cycle.

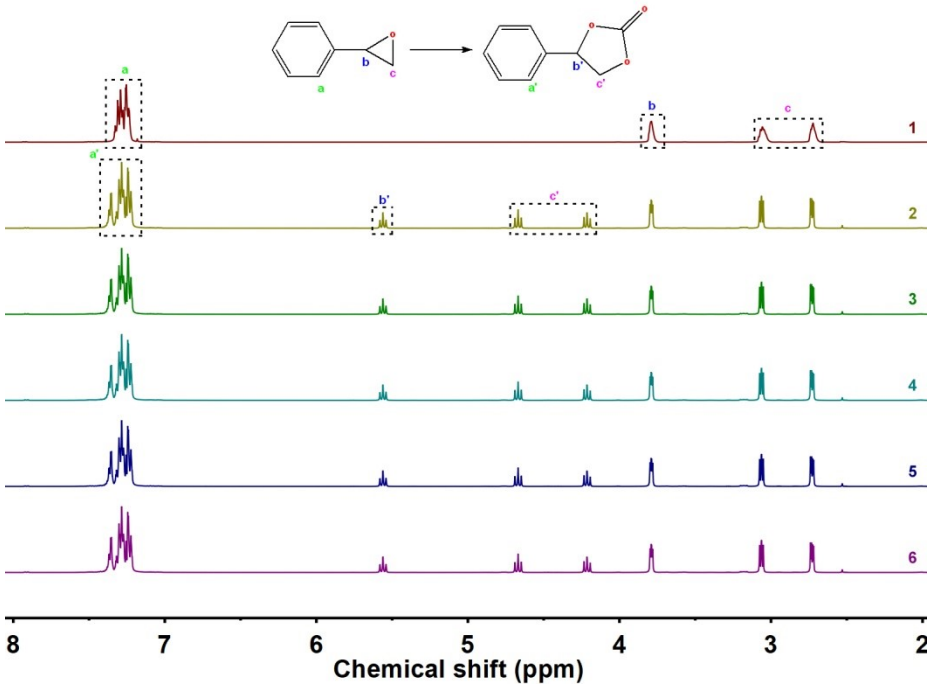

Fig. S16 The ^{1}H NMR spectrum (in $CDCl_3$) of a solution after the cycloaddition of CO_2 with 2-phenyloxirane: 1) without catalyst HNUST-17, 2) first cycle, 3) second cycle, 4) third cycle, 5) fourth cycle and 6) fifth cycle.

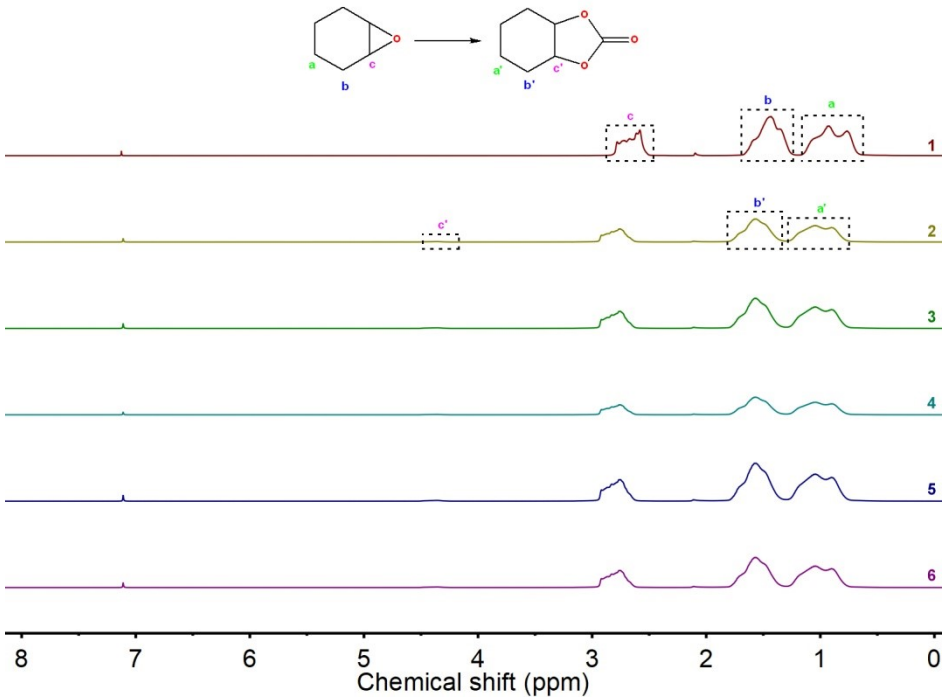

Fig. S17 The ^{1}H NMR spectrum (in $CDCl_3$) of a solution after the cycloaddition of CO_2 with cyclohexene oxide: 1) without catalyst HNUST-17, 2) first cycle, 3) second cycle, 4) third cycle, 5) fourth cycle and 6) fifth cycle.

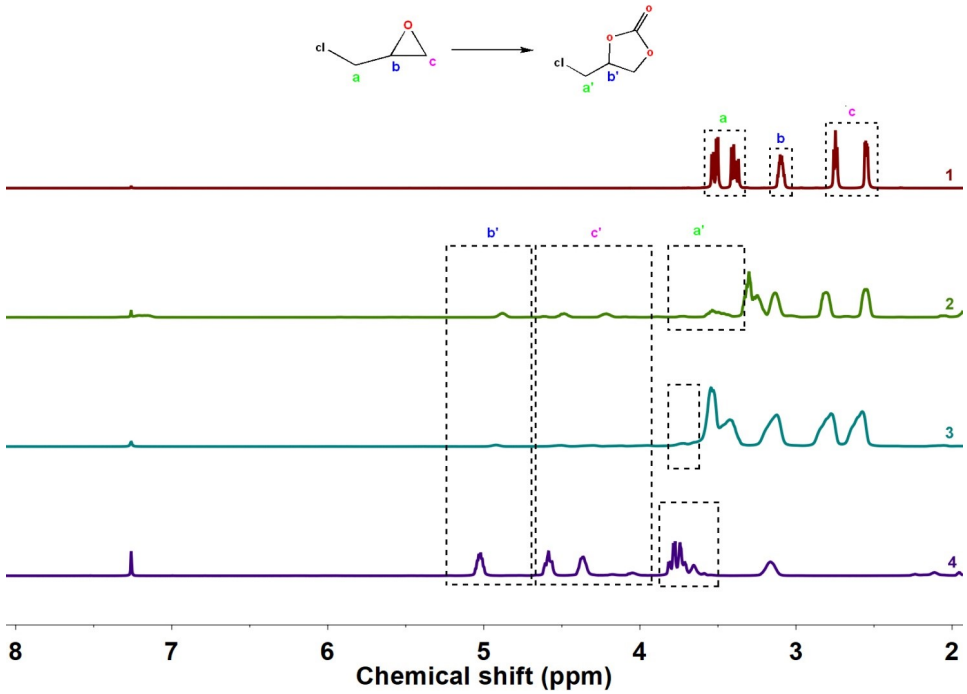

Fig. S18 The ^{1}H NMR spectrum (in $CDCl_3$) of a solution after the controlled experiments for cycloaddition of CO_2 with 2-(chloromethyl)oxirane. 1) without catalyst HNUST-17, 2) catalyzed by the cocatalyst TBAB alone, 3) catalyzed by both HNUST-17 and TBAB available at the same conditions.

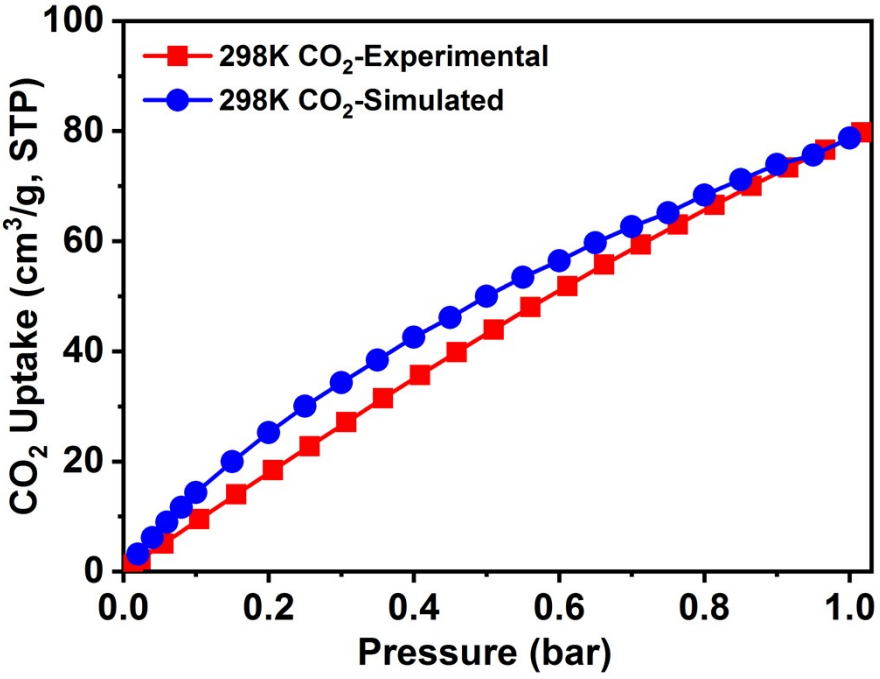

Fig. S19 Comparison of CO_2 adsorption isotherms of HNUST-17 at 298 K up to 1 bar between GCMC simulated and experimental data.

Table S1. Crystal data and structure refinement for HNUST-17

Identification code	**HUNST-17**
CCDC number	2348601

Empirical formula	$C_{35}H_{22}Cu_2N_4O_{11}$
Formula weight	801.64
Temperature	273 K
Wavelength	0.71073 Å
Crystal system	Cubic
Space group	Im-3m (229)
Unit cell dimensions.	$a = b = c$ = 36.138(9) Å, $\alpha = \beta = \gamma$ = 90°
Volume	47163(31) Å^3
Z	24
Density (calculated)	0.677 g·cm^3
Absorption coefficient	0.813 mm^{-1}
F(000)	9720.0
Crystal size	0.18 × 0.2 × 0.14 mm^3
2theta range for data collection	4.218 to 50.746
Limiting indices	-43 <= h <= 41, -43 <= k <= 43, -41 <= l <= 43
Reflections collected / unique	154811/2940 [R_{int} = 0.1442]
Completeness	99.5% (2theta = 52.00°)
Absorption correction	Semi-empirical from equivalents
Refinement method	Full-matrix least-squares on F^2
Data /restraints / parameters	4072/188/207
Goodness-of-fit on F^2	1.925
Final R indices [I>2sigma(I)]	R_1 = 0.1271, w$R_2{}^a$ = 0.3742
R indices (all data)	R_1 = 0.1577, w$R_2{}^a$ = 0.4283
Largest diff. peak and hole	2.04/-1.45 e. Å^{-3}

^{a} $R_1 = \Sigma||F_o| - |F_c||/|F_o|$; $wR_2 = [\Sigma w(\Sigma F_o^2 - F_c^2)^2/\Sigma w(F_o^2)^2]^{1/2}$.

Table S2. Lennard-Jones parameters of HNUST-17

Atom Type	ε/k_B (K)	σ (Å)	Atom Type	ε/k_B (K)	σ (Å)
H	22.141	2.571	C	52.836	3.431
O	30.192	3.118	N	34.721	3.261

Cu	2.516	3.114			

Table S3. Lennard-Jones parameters and charges of adsorbates

Atom Type	ε/k_B (K)	σ (Å)	q (e)
CO2_O	85.671	3.017	-0.3256
CO2_C	29.933	2.745	0.6512

Table S4. Comparison of catalytic activity of HNUST-17 for cycloaddition of CO_2 and 2-(chloromethyl)oxirane with those of some literature-reported MOF catalysts

Entry	Catalyst	Catalytic conditions	Conversion	TON[a]	Ref

			(%)		
1	HNUST-17	substrate (20 mmol), catalyst (9 mg), TBAB (1% mmol based on epoxides), 1 bar CO_2 (balloon pressure), 80 °C and 24 h.	>98.5	1755	This work
2	$[Cu_6(TABAB)_4(DABCO)_3]_n$	substrate (20 mmol), catalyst (0.02 mmol), 8 bar CO_2, 80 °C and 24 h.	93	NA[b]	S4
3	HNUST-9	substrate (20 mmol), catalyst (9 mg), TBAB (1% mmol based on epoxides), CO_2 (balloon pressure), 80 °C and 48 h.	>99.9	1332	S5
4	$[Co_2(tzpa)(OH)]_n$	substrate (20 mmol), catalyst (0.2 mmol), TBAB (2 mmol), 1 bar CO_2, 25 °C, 48 h.	93.8	NA	S6
5	$[Cu_4(C_{57}H_{32}N_{12})(COO)_8]_n$	substrate (20 mmol), catalyst (0.2 mmol %), TBAB (10 mol %), 1 bar CO_2, 25 °C, 48 h.	85	177	S7
6	$[Sr(BDPO)_{0.5}]_n$	substrate (28.6 mmol), catalyst (0.84 % mmol), TBAB (3.5% mmol), 1 bar CO_2, 25 °C and 48 h.	98.5	117.4	S8
7	$[(C_2NH_8]_6(Cd_3L)]_n$	substrate (5 mmol), catalyst (5 mg, 0.002 mmol based on Lewis acid sites), TBAB (0.16 g, 0.5 mmol), 1 bar CO_2, 80 °C and 24 h.	99	2745	S9
8	JUC-1000	substrate (20.0 mmol), catalyst (0.25 mol% per exposed copper site), TBABr (0.65 g), at room temperature 1 bar CO_2, 25 °C and 48 h.	96	NA	S10

[a] Turnover number (TON) = [mmol (product)]/[mmol (Lewis acid sites)]. [b] NA = Not available.

Table S5. Comparison of the CO_2 sorption properties of HNUST-17 with those of some literature-reported MOFs with various surface areas

Entry	MOF	BET (m^2/g)	CO_2 uptake capacities	Q_{st} (kJ/mol)	Selectivity (CO_2/N_2, CO_2/CH_4)	Ref
1	HNUST-17	2575	145.41 and 79.75 $cm^3 \cdot g^{-1}$ at 273 K and 298 K under 1 bar; 24.49 and 18.80 $mmol \cdot g^{-1}$ under 30 bar at 273 K and 298 K.	25.4	207 and 8.0 for CO_2/N_2 and CO_2/CH_4 at 273 K.	This work
2	HNUST-7	2804	121.44 and 68.05 $cm^3 \cdot g^{-1}$ at 273 and 298 K under 1 bar; 26.1 and 19.4 $mmol \cdot g^{-1}$ under 30 bar at 273 and 298 K.	24.8	22.39 and 6.92 for CO_2/N_2 and CO_2/CH_4 at 273 K.	S11
3	HNUST-8	2801	144.76 and 78.36 $cm^3 \cdot g^{-1}$ at 273 and 298 K under 1 bar; 22.42 and 19.5 $mmol \cdot g^{-1}$ under 30 bar at 273 and 298 K.	24.9	16.2 and 5.0 for CO_2/N_2 and CO_2/CH_4 at 298 K.	S12
4	HNUST-2	2366	21.6 and 18.1 $mmol \cdot g^{-1}$ under 20 bar at 273 and 298 K.	23.5	22.9 and 4.9 for CO_2/N_2 and CO_2/CH_4 at 298 K.	S13
5	HHU-1	2290	114.6 and 66.8 $cm^3 \cdot g^{-1}$ at 273 K and 298 K under 1 bar; 21.53 $mmol \cdot g^{-1}$ under 40 bar at 298 K.	27.7	140 for CO_2/N_2 at 273 K.	S14
6	NJU-Bai22	2221	72.9 $cm^3 \cdot g^{-1}$ at 298 K under 1 bar; 21.3 $mmol \cdot g^{-1}$ under 40 bar at 298 K.	25.6	81 and 6.7 for CO_2/N_2 and CO_2/CH_4 at 298 K.	S15
7	NTU-105	3543	168.3 $cm^3 \cdot g^{-1}$ (36.7 wt%) at 273 K and 1 bar.	NA[a]	NA	S16
8	$(In_2X)(Me_2NH_2)_2$, H_8X=tetrakis [(3,5-dicarboxyphenoxy)methyl] methane	1555	99.7 and 56.2 $cm^3 \cdot g^{-1}$ at 273 K and 298 K under 1 bar.	21.14	250 for CO_2/N_2 at 273 K.	S17

9	CPM-33a	996	137.2 and 73.6 $cm^3 \cdot g^{-1}$ at 273 K and 298 K under 1 bar.	22.5	NA	S18
10	CPM-33b	808	173.9 and 126.4 $cm^3 \cdot g^{-1}$ at 273 K and 298 K under 1 bar.	25.0	NA	S18
11	CPM-33c	805	134.2 and 88.5 $cm^3 \cdot g^{-1}$ at 273 K and 298 K under 1 bar.	21.5	NA	S18
12	Bio-MOF-11	1040	91.1 $cm^3 \cdot g^{-1}$ at 298 K under 1 bar.	45.0	81 and 75 for CO_2/N_2 at 273 K and 298 K.	S19
13	CuBTTri	1770	85.0 $cm^3 \cdot g^{-1}$ at 298 K under 1 bar.	90.0	NA	S20
14	$[Ba_2(BDPO)]$	487	75.85 and 52.92 $cm^3 \cdot g^{-1}$ at 273 K and 298 K under 1 bar.	32.7	12.3 for CO_2/CH_4 at 298 K.	S21
15	MIL-100	1900	18 $mmol \cdot g^{-1}$ at 303 K under 48.7 bar.	62	NA	S22
16	RMOF-11	2096	14.7 $mmol \cdot g^{-1}$ at 298 K under 35 bar.	NA	NA	S23
17	IRMOF-3	2160	18.7 $mmol \cdot g^{-1}$ at 298 K under 35 bar.	NA	NA	S23
18	IRMOF-6	2516	19.5 $mmol \cdot g^{-1}$ at 298 K under 35 bar.	NA	NA	S23
19	MOF-5	3800	21.7 $mmol \cdot g^{-1}$ at 298 K under 35 bar.	NA	NA	S23
20	HKUST-1	1781	10.7 $mmol \cdot g^{-1}$ at 298 K under 35 bar.	30	NA	S23/ 24
21	MOF-177	4508	33.5 $mmol \cdot g^{-1}$ at 298 K under 35 bar.	NA	NA	S23
22	RMOF-1	2833	21.7 $mmol \cdot g^{-1}$ at 298 K under 35 bar.	NA	NA	S23
23	MIL-101	4230	40.0 $mmol \cdot g^{-1}$ at 303 K under 50 bar.	NA	NA	S22
24	MOF210	5850	54.5 $mmol \cdot g^{-1}$, at 298 K under 50 bar	NA	NA	S25

25	MOF200	6400	54.5 mmol·g^{-1}, at 298 K under 50 bar	NA	NA	S25

[a] NA = Not available.

References

S1. Y. Bae, K. L. Mulfort, H. Frost, P. Ryan, S. Punnathanam, L. J. Broadbelt, J. T. Hupp and R. Q. Snurr, Separation of CO_2 from CH_4 using mixed-ligand metal-organic frameworks, *Langmuir*, 2008, *24*, 8592-8598.

S2. J. Rouquerol, P. Llewellyn and F. Rouquerol, Is the bet equation applicable to microporous adsorbents? *Stud. Surf. Sci. Catal.*, **2007**, *160* ,49-56.

S3. K. S. Walton and R. Q. Snurr, Applicability of the BET method for determining surface areas of microporous metal-organic frameworks, *J. Am. Chem. Soc.*, **2007**, *129*, 8552-8556.

S4. Sandeep Singh Dhankhar, Rajesh Das, Bharat Ugale, Renjith S. Pillai, and C. M. Nagaraja, Chemical fixation of CO_2 under solvent and Co-catalyst-free conditions using a highly porous two-fold interpenetrated Cu(II)-metal-organic framework, *Cryst. Growth Des.*, 2021, *21*, 1233-1241.

S5. J. X. Liao, W. J. Zeng, B. S. Zheng, X. Y. Cao, Z. X. Wang, G. Y. Wang and Q. Y. Yang, Highly efficient CO_2 capture and conversion of a microporous acylamide functionalized rht-type metal-organic framework, *Inorg. Chem. Front.*, 2020, *7*, 1939-1948.

S6. H.-H. Wang, L. Hou, Y.-Z. Li, C.-Y. Jiang, Y.-Y. Wang and Z. H. Zhu, Porous MOF with highly efficient selectivity and chemical conversion for CO_2, *ACS Appl. Mater. Interfaces*, 2017, *9*, 17969-17976.

S7. P.-Z. Li, X.-J. Wang, J. Liu, J. S. Lim, R. Zou and Y. Zhao, A Triazole-containing metal-organic framework as a highly effective and substrate size-dependent catalyst for CO_2 conversion, *J. Am. Chem. Soc.*, 2016, *138*, 2142-2145.

S8. X.-Y. Li, Y.-Z. Li, Y. Yang, L. Hou, Y.-Y. Wang and Z. H. Zhu, Efficient light hydrocarbon separation and CO_2 capture and conversion in a stable MOF with oxalamide-decorated polar tubes, *Chem. Commun.*, 2017, *10,* 12970-12973.

S9. B.-B. Lu, W. Jiang, J. Yang, Y.-Y. Liu and J.-F. Ma, Resorcin[4]arene-based microporous metal-organic framework as an efficient catalyst for CO_2 cycloaddition with epoxides and highly selective luminescent sensing of $Cr_2O_7^{2-}$, *ACS Appl. Mater. Interfaces*, 2017, *9*, 39441-39449.

S10. H. M. He, Q. Sun, W. Y. Gao, J. A. Perman, F. X. Sun, G. S. Zhu, B. Aguila, K. Forrest, B. Space and S. Q. Ma, A stable metal-organic framework featuring a local buffer environment for carbon dioxide fixation, *Angew. Chem. Int. Ed.*, 2018, *57*, 4657-4662.

S11. B. S. Zheng, L. Huang, X. Y. Cao, S. H. Shen, H. F. Cao, C. Hang, W. J. Zeng and Z. X. Wang, A highly porous acylamide decorated MOF-505 analogue exhibiting high and selective CO_2 gas uptake capability, *CrystEngComm.*, 2018, *20*, 1874-1881.

S12. B. Zheng, X. Luo, Z. Wang, S. Zhang, R. Yun, L. Huang, W. Zeng and W. Liu, An unprecedented water stable acylamide-functionalized metal-organic framework for highly efficient CH_4/CO_2 gas storage/separation and acid-base cooperative catalytic activity, *Inorg. Chem. Front.*, 2018, 5, 2355-2363.

S13. Z. X. Wang, B. S. Zheng, H. T. Liu, P. G. Yi, X. F. Li, X. Y. Yu and R. R. Yun, A highly porous 4,4-paddlewheel-connected NbO-type metal-organic framework with a large gas-uptake capacity, *Dalton Trans*., 2013, *42*, 11304-11311.

S14. Z. Y. Lu, J. F. Zhang, H. Y. He, L. T. Du and C. Hang, A mesoporous (3, 36)-connected txt-type metal–organic framework constructed by using a naphthyl-embedded ligand exhibiting high CO_2 storage and selectivity, *Inorg. Chem. Front.*, 2017, *4*, 736-740.

S15. Z. Y. Lu, J. F. Bai, C. Hang, F. Meng, W. L. Liu, Y. Pan and X. Z. You, The utilization of amide groups to expand and functionalize metal-organic frameworks simultaneously, *Chem-Eur. J.*, 2016, *22*, 6277-6285.

S16. X.-J. Wang, P.-Z. Li, Y. F. Chen, Q. Zhang, H. C. Zhang, X. X. Chan, R. Ganguly, Y. X. Li, J. W. Jiang, Y. L. Zhao, A rationally designed nitrogen-rich metal-organic framework and its exceptionally high CO_2 and H_2 uptake capability, *Sci*. *Rep*., 2013, *3*, 1149.

S17. Z.-J. Lin, Y.-B. Huang, T.-F. Liu, X.-Y. Li and R. Cao, Construction of a polyhedral metal-organic framework via a flexible octacarboxylate ligand for gas adsorption and separation, *Inorg*. *Chem*., 2013, *52*, 3127-3132.

S18. X. Zhao, X. H. Bu, Q.-G. Zhai, H. Tran and P. Y. Feng, Pore space partition by symmetry-matching regulated ligand insertion and dramatic tuning on carbon dioxide uptake, *J. Am*. *Chem*. *Soc*., 2015, *137*, 1396-1399.

S19. J. An, S. J. Geib, N. Rosi, High and selective CO_2 uptake in a cobalt adeninate metal-organic framework exhibiting pyrimidine- and amino-decorated pores, *J. Am. Chem. Soc*., 2010, *132*, 38-39.

S20. A. Demessence, D. M. D'Alessandro, M. L. Foo, J. R. Long, Strong CO_2 binding in a water-stable, triazolate-bridged metal-organic framework functionalized with ethylenediamine, *J. Am. Chem. Soc*., 2009, *131*, 8784-8786.

S21. X.-Y. Li, L.-N. Ma, Y. Liu, L. Hou, Y.-Y. Wang, Z. H. Zhu, Honeycomb metal-organic framework with Lewis acidic and basic bifunctional sites: selective adsorption and CO_2 catalytic fixation, *ACS Appl. Mater. Interfaces*, 2018, *10*, 13, 10965-10973.

S22. P. L. Llewellyn, S. Bourrelly, C. Serre, A. Vimont, M. Daturi, L. Hamon, G. De Weireld, J.-S. Chang, D.-Y. Hong, Y.K. Hwang, S.H. Jhung, G. Ferey, High Uptakes of CO_2 and CH_4 in Mesoporous Metal-organic frameworks MIL-100 and MIL-101, *Langmuir*, 2008, *24*, 7245-7250.

S23. A. R. Millward, O. M. Yaghi, Metal-organic frameworks with exceptionally high capacity for storage of carbon dioxide at room temperature, *J. Am. Chem. Soc*., 2005, *127*, 17998-17999.

S24. Z.J. Liang, M. Marshall, A.L. Chaffee, CO_2 adsorption-based separation by metal organic framework (Cu-BTC) versus Zeolite (13X), *Energy Fuels*, 2009, *23*, 2785-2789.

S25. H. Furukawa, N. Ko, Y. Bok Go, N. Aratani, S. B. Choi, E. Choi, A. Ö. Yazaydin, R. Q. Snurr, M. O'Keeffe, J. Kim, O. M. Yaghi, Ultrahigh porosity in metal-organic frameworks, *Science*, 2010, *329*, 424.